In vivo hyperspectral confocal fluorescence imaging to determine pigment localization and distribution in cyanobacterial cells

Wim F. J. Vermaas*†, Jerilyn A. Timlin‡, Howland D. T. Jones‡, Michael B. Sinclair‡, Linda T. Nieman‡§, Sawsan W. Hamad*, David K. Melgaard‡, and David M. Haaland‡

*School of Life Sciences and Center for Bioenergy and Photosynthesis, Arizona State University, Box 874501, Tempe, AZ 85287-4501; and ‡Sandia National Laboratories, MS0895, Albuquerque, NM 87185

Edited by Elisabeth Gantt, University of Maryland, College Park, MD, and approved January 25, 2008 (received for review August 27, 2007)

Hyperspectral confocal fluorescence imaging provides the opportunity to obtain individual fluorescence emission spectra in small (≈0.03-μm^3) volumes. Using multivariate curve resolution, individual fluorescence components can be resolved, and their intensities can be calculated. Here we localize, *in vivo*, photosynthesis-related pigments (chlorophylls, phycobilins, and carotenoids) in wild-type and mutant cells of the cyanobacterium *Synechocystis* sp. PCC 6803. Cells were excited at 488 nm, exciting primarily phycobilins and carotenoids. Fluorescence from phycocyanin, allophycocyanin, allophycocyanin-B/terminal emitter, and chlorophyll *a* was resolved. Moreover, resonance-enhanced Raman signals and very weak fluorescence from carotenoids were observed. Phycobilin emission was most intense along the periphery of the cell whereas chlorophyll fluorescence was distributed more evenly throughout the cell, suggesting that fluorescing phycobilisomes are more prevalent along the outer thylakoids. Carotenoids were prevalent in the cell wall and also were present in thylakoids. Two chlorophyll fluorescence components were resolved: the short-wavelength component originates primarily from photosystem II and is most intense near the periphery of the cell; and the long-wavelength component that is attributed to photosystem I because it disappears in mutants lacking this photosystem is of higher relative intensity toward the inner rings of the thylakoids. Together, the results suggest compositional heterogeneity between thylakoid rings, with the inner thylakoids enriched in photosystem I. In cells depleted in chlorophyll, the amount of both chlorophyll emission components was decreased, confirming the accuracy of the spectral assignments. These results show that hyperspectral fluorescence imaging can provide unique information regarding pigment organization and localization in the cell.

cyanobacteria | photosynthetic pigments | multivariate curve resolution

Cyanobacteria convert light energy to chemical energy by means of photosynthesis, using water as a source of electrons for CO_2 reduction and O_2 production. A key part of the photosynthesis process is light absorption (harvesting) by pigments, followed by excitation transfer to reaction center chlorophyll (Chl) *a* of photosystems (PS) II and I (1). These processes take place in thylakoid membranes that in cyanobacteria generally form an extensive internal membrane complex of several layers along the periphery of the cytoplasm, with thylakoids found less frequently toward the center of the cell (2).

The pigments associated with the photosynthetic apparatus are bound to thylakoid proteins, modifying their spectral properties and providing a spatial distribution that aids in the efficiency of light harvesting and energy transfer to reaction center Chls. Pigments bound to integral membrane proteins in reaction center complexes in thylakoids of cyanobacteria include Chl *a* [≈40 per PS II (3) and ≈100 per PS I (4)] and carotenoids; the latter act in photoprotection and ^{3}Chl quenching but do not effectively transfer energy to Chl in cyanobacterial PS II (5). Carotenoids are also present in the outer cell membrane and cytoplasmic membrane of cyanobacteria, whereas Chl is not (6, 7). Additional light-harvesting capability, primarily for PS II, is provided by phycobilisomes, which are pigment-binding complexes in the cytoplasm that associate with thylakoids to enable energy transfer to Chl (8, 9). Phycocyanin (PC), allophycocyanin (APC), and allophycocyanin-B (APC-B) are the main phycobilisome pigments in *Synechocystis* sp. PCC 6803 (10).

Chl and phycobilisome pigments fluoresce at room temperature with spectral maxima in the 640- to 700-nm range. PC emits fluorescence with an ≈650-nm maximum, APC at 665 nm, and APC-B at 675 nm, and the main emission wavelength of Chl is at 685 nm (11). Phycobilisomes are highly fluorescent in isolated form, but the fluorescence yield is decreased in intact systems because *in vivo* the excitation energy is transferred efficiently from PC to APC to APC-B or to long-wavelength APC associated with the ApcE protein (terminal emitter) (12) and eventually to Chl in the thylakoid membranes.

Much is known regarding cyanobacterial cell architecture and thylakoid organization (2, 13–15), the structure of individual pigment-binding complexes (16, 17), the distribution of photosynthetic complexes in fixed thylakoid membranes (18), and the ability of phycobilisomes to dynamically associate with photosynthetic complexes in the membrane (19–21). However, photosynthetic pigments and their interactions have not yet been visualized distinctly *in vivo* because of their spectral overlap. Spectral congestion (fluorescence emission maxima that are different by <20–30 nm) is common in photosynthetic systems that depend on spectral overlap for efficient energy transfer and presents a major problem in data analysis/interpretation. Confocal laser scanning microscopy coupled with spectral imaging techniques has the potential to visualize photosynthetic pigments even amidst spectral overlap. However, because of low spectral resolution of current commercial instrumentation and the absence of methods available for robust analysis of spectrally and spatially overlapped spectral images, application of this technique has been limited to systems with relatively few fluorescent pigments that are spectrally distinct and spatially isolated (22). The recent development of a high-resolution hyperspectral confocal fluorescence imaging microscope (23) and correspond-

Author contributions: W.F.J.V., J.A.T., H.D.T.J., M.B.S., and D.M.H. designed research; W.F.J.V., J.A.T., H.D.T.J., M.B.S., L.T.N., S.W.H., and D.M.H. performed research; W.F.J.V., J.A.T., H.D.T.J., M.B.S., S.W.H., D.K.M., and D.M.H. contributed new reagents/analytic tools; W.F.J.V., J.A.T., H.D.T.J., M.B.S., L.T.N., S.W.H., D.K.M., and D.M.H. analyzed data; and W.F.J.V., J.A.T., H.D.T.J., and D.M.H. wrote the paper.

The authors declare no conflict of interest.

This article is a PNAS Direct Submission.

†To whom correspondence should be addressed. E-mail: wim@asu.edu.

§Present address: Department of Biomedical Engineering, University of Texas M. D. Anderson Cancer Center, Houston, TX 77030.

This article contains supporting information online at www.pnas.org/cgi/content/full/0708090105/DC1.

© 2008 by The National Academy of Sciences of the USA

ing robust multivariate curve resolution (MCR) algorithms (24–28) provide a unique opportunity to reliably resolve pigments with rather similar fluorescence emission spectra in a living cell with diffraction-limited spatial resolution (≈250 × 250 × 600 nm). By using MCR, spectra representing pure fluorescent components can be extracted without reference spectra, provided that such components are not present in the same ratio relative to each other in all voxels. This approach allows a detailed determination of pure individual fluorescent components and their relative intensities in three dimensions within a single cell.

Synechocystis sp. PCC 6803 is a model cyanobacterium with a known genome sequence and a facile and reliable transformation system (29, 30). Mutants lacking genes for specific photosystems or pigment biosynthesis pathways have been created. One mutant strain used in this study lacks the genes for PsaA and PsaB, the major subunits of PS I, with which ≈75% of the Chl in the cell is associated (31). Consequently, the PS I-less strain contains only ≈25% of the usual amount of Chl *a*, without affecting the phycobilisome content. In addition, we use a strain that lacks *chlL*, which codes for a component of the light-independent NADPH/protochlorophyllide oxidoreductase (32). As a consequence, this strain cannot synthesize Chl in darkness, but Chl synthesis can occur in the light because of the presence of a light-dependent protochlorophyllide oxidoreductase (33). Moreover, we have used the double mutant (PS I-less/ChlL-less) (34) and the wild-type strain in this study. Together, these strains represent a collection with different pigment compositions and properties and allow validation of spectral assignments.

Results

Hyperspectral Imaging of Intact *Synechocystis* Cells. Using 488-nm laser excitation, fluorescence was elicited from intact, live *Synechocystis* cells of three strains grown under normal and light-activated heterotrophic growth (LAHG) conditions, and the fluorescence spectra were measured on a 120 × 120 × 300 nm (LxWxH) voxel (3D pixel) spacing, i.e., approximately half of the diffraction-limited spatial resolution. Data from these independent images were combined into a single composite image (≈100 spectra for each cell, tens of cells per imaged area, and multiple images per strain) to facilitate analysis. Using MCR algorithms (24–28), a single set of six independently varying pure emission spectra was found. These pure spectra were used to achieve an excellent least-squares fit (99.97% of the non-noise spectral variance explained) to all of the images of intact *Synechocystis* presented. These pure-component emission spectra (Fig. 1*A*) represent five major fluorescence components with emission maxima between 645 and 700 nm, plus one low-intensity component at shorter emission wavelength with resonance Raman bands superimposed. Two separate Chl components were resolved, one (Chl-698) red-shifted relative to the other (Chl-685), representing predominantly PS I- and PS II-associated Chl, respectively. The fact that these two factors were resolved as separate components in MCR analysis indicates that they varied in intensity and location relative to each other in different pixels: Two fluorescence components that covary in their amplitudes in all locations will not be resolved as separate MCR components. Fig. 1*B Upper* displays the MCR fit for a single pixel from an image of wild-type cells, and Fig. 1*B Lower* shows (on an expanded scale) the spectral residuals remaining after the fit. The reproducibility of the MCR approach across multiple cells is illustrated in supporting information (SI) Fig. 5, indicating that intensity and distribution patterns of components were rather uniform among cells of a specific strain or growth condition.

To determine which pigments are excited at 488 nm, fluorescence spectra of whole cells were obtained by using a conventional fluorimeter (SI Fig. 6). At 488 nm primarily phycobilisomes and carotenoids are excited and Chl *a* absorbs poorly. Part of the longer-wavelength Chl emission observed upon 488-nm excitation originates by energy transfer from phycobilisomes or carotenoids.

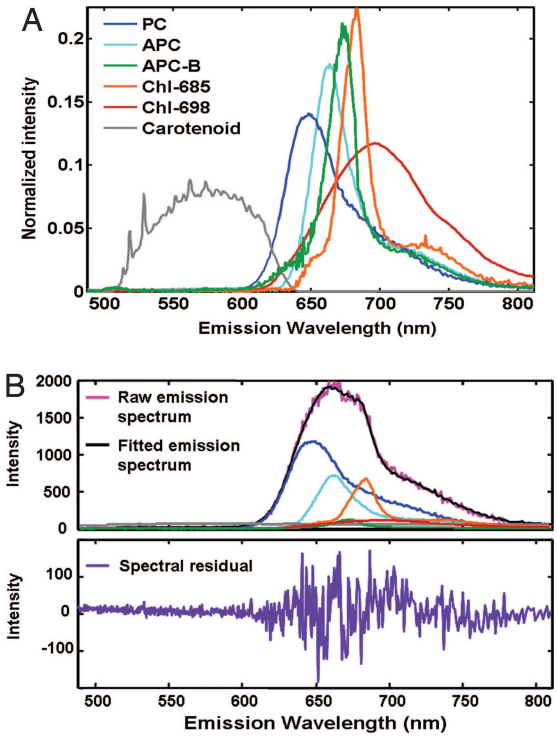

Fig. 1. MCR analysis of a single optical section from a 3D hyperspectral image of live wild-type *Synechocystis* cells. (*A*) Mathematically extracted pure-component spectra of fluorescent components in *Synechocystis* using the pure emission spectra obtained from the composite image in SI Fig. 5. The spectra were normalized to unit length as required for MCR algorithm stability. (*B Upper*) Fit between the measured and modeled emission spectrum for a single voxel. Colors of contributing pure-component spectra are as in *A*. (*B Lower*) Difference between the calculated and observed signal for this same voxel, which represents the image voxel with the poorest fit.

Fig. 2*A* presents fluorescence intensities of individual components in a two-dimensional plane through a typical wild-type cell. Fig. 2*B* presents the relative intensities of fluorescence components obtained from an average of 10 evenly spaced cross-cuts through the wild-type cell shown in Fig. 2*A*. Fig. 2*C* represents the standard deviation of the 10 cross-cuts indicating that these distributions are statistically significant for nearly all components throughout the cell at the $\alpha = 0.05$ significance level. Only the distribution of the very weak APC-B component is not always statistically significant throughout the width of the cells (see SI Fig. 7 for a direct comparison of the mean distributions and two standard deviation levels). Similar trends are observed for the population of 10 wild-type cells (first row in SI Fig. 5) based on 10 cross-cuts through each of the 10 cells (100 cross-cuts total; data not shown), although the variable cell size adds slightly to the variance of these distributions across all of the cells. Chl fluorescence components were present where thylakoids are expected (2), with the 698-nm component more homogeneously distributed than the 685-nm component, which more closely followed the distribution of the PC and APC components along the periphery of the cell. However, the relative intensity near the center of the cell was slightly higher for Chl-685 than for PC or APC. The ratio of Chl-698 to PC/APC fluorescence within a cell varied by about a factor of two: Thylakoids near the center of the cell had the highest relative

PLANT BIOLOGY

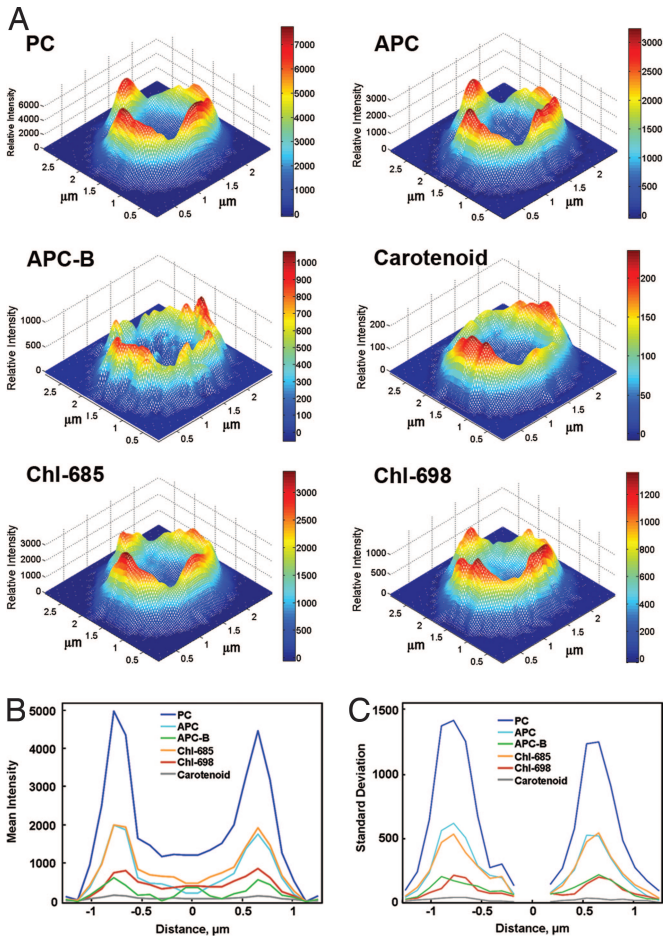

Fig. 2. Fluorescence distribution in *Synechocystis* cells. (*A*) Mesh plots of fluorescence intensity vs. spatial distribution of the six components (Fig. 1*A*) in a wild-type *Synechocystis* cell. (*B*) Mean intensities from 10 equally spaced cross-cuts through the center of the cell detailed in *A*. (*C*) Standard deviations for each component obtained from the 10 cross-cuts. For clarity, *A* and *B* are shown on different scales.

Chl-698 intensity, whereas those near the periphery had the lowest ratio.

The weak APC-B fluorescence was unevenly distributed along the periphery. The APC-B component is very susceptible to Poisson noise in the spectral data because this component had a low intensity and was spectrally similar to the more intense APC and Chl-685 components. Error analysis indicated that much of the change in the APC-B fluorescence intensity in neighboring voxels was due to noise in the data (data not shown), providing a note of caution when resolving spectrally weak components in the presence of stronger spectrally adjacent components. For this reason the 95% confidence limit is considered when interpreting the results of this study.

One unexpected spectral component was the weak carotenoid fluorescence spectrum with resonance Raman bands superimposed. Although this component contributed only ≈0.1% of the total spectral variance, it was easily identified as an independent component because of its spectral dissimilarity and distinct spatial location. The resonance Raman band positions and relative intensities were in line with those reported for carotenoids in PS I and PS II (35, 36) and those of pure β-carotene in solution (data not shown).

Chlorophyll Depletion. The 488-nm excitation light is absorbed primarily by phycobilisomes and carotenoids, with subsequent energy transfer to Chl. Therefore, the pigment absorbing the light is not necessarily the complex emitting the corresponding fluorescence. To evaluate this potential issue, a mutant was used that lacks *chlL* and thus can synthesize Chl in the light but not in darkness (32). Growth of this mutant under LAHG conditions (15 min of light per day to activate a blue-light receptor needed to maintain long-term viability of the cells) leads to depletion of Chl levels to 5–10% of that found in wild type (33). However, as shown in SI Fig. 8, the distribution of thylakoids in the cell is similar to that of cells grown under continuous light or that of the wild-type or PS I-less strain.

Fig. 3 presents a mesh plot of the six fluorescence components in the wild type and two mutant strains: the PS I-less strain grown in continuous light and the ChlL-less strain grown under LAHG conditions. To better visualize relative intensities of the various components displayed in Fig. 3, the total intensity of the fluorescence in each voxel was taken as 100%. A corresponding plot of the same cells with absolute intensities displayed for each component is presented in SI Fig. 9 for comparison. The pattern of the PC, APC, and APC-B distribution in the LAHG-grown ChlL-less cell shown here was qualitatively similar to that in the continuous-light-grown wild-type cell although the dip in the middle of the cell was less pronounced because of the low Chl fluorescence intensity of the ChlL-less cell. The similar distribution of phycobilin fluorescence upon Chl depletion indicated that energy transfer from phycobilisomes to Chl in the wild type did not unduly distort the distribution of phycobilisomes relative to phycobilin emission. The fluorescence distribution in wild-type cells grown under LAHG conditions (wild type retains a normal amount of Chl under these conditions) vs. in continuous light was similar (SI Fig. 5), indicating that growth under LAHG conditions does not greatly alter the pigment distribution in cells.

Photosystem I Fluorescence. In another cyanobacterium, *Synechococcus* sp. PCC 7942, a radial asymmetry of PS I was suggested based on immunocytochemistry, with PS I localized primarily near or at the periphery of the cell (18). In *Synechocystis*, Chl with long-wavelength fluorescence emission is associated primarily with PS I (37), and the distribution of the Chl-698 component is more centrally located within the cell compared with the Chl-685 component (Figs. 2 and 3). To further explore this apparent discrepancy, a PS I-less mutant (31) was investigated (Fig. 3). As shown in Fig. 3 and SI Table 1, the Chl-698 component in the PS I-less strain was so low as to be indistinguishable from the noise for most voxels, strengthening both the assignment of the Chl-698 component to PS I-associated Chl and the confidence in the quality of the resolution of the pure-component spectra.

Variance. Because the MCR results from composite images (see, e.g., SI Fig. 5) provide component concentrations for every cell-related pixel in the image, statistical analysis of variance decompositions can be performed to better understand the sources of variance in the image on a component-by-component basis, e.g., pixel-to-pixel variance within a cell vs. cell-to-cell variance within a strain (or growth condition) vs. strain-to-strain variance. Fig. 4 shows this analysis of variance for the composite image in SI Fig. 5. Fig. 4 demonstrates that the pixel-to-pixel variance is a large source of variance in the composite image because of the often large intensity variations for most components from the edge to the center of the cells. Importantly, except for the dominant PC and weak APC-B component, the strain-to-strain variances dominate cell-to-cell variances, indicating that observed differences are due mainly to differences in the strain or LAHG vs. continuous light growth rather than cell-to-cell variation.

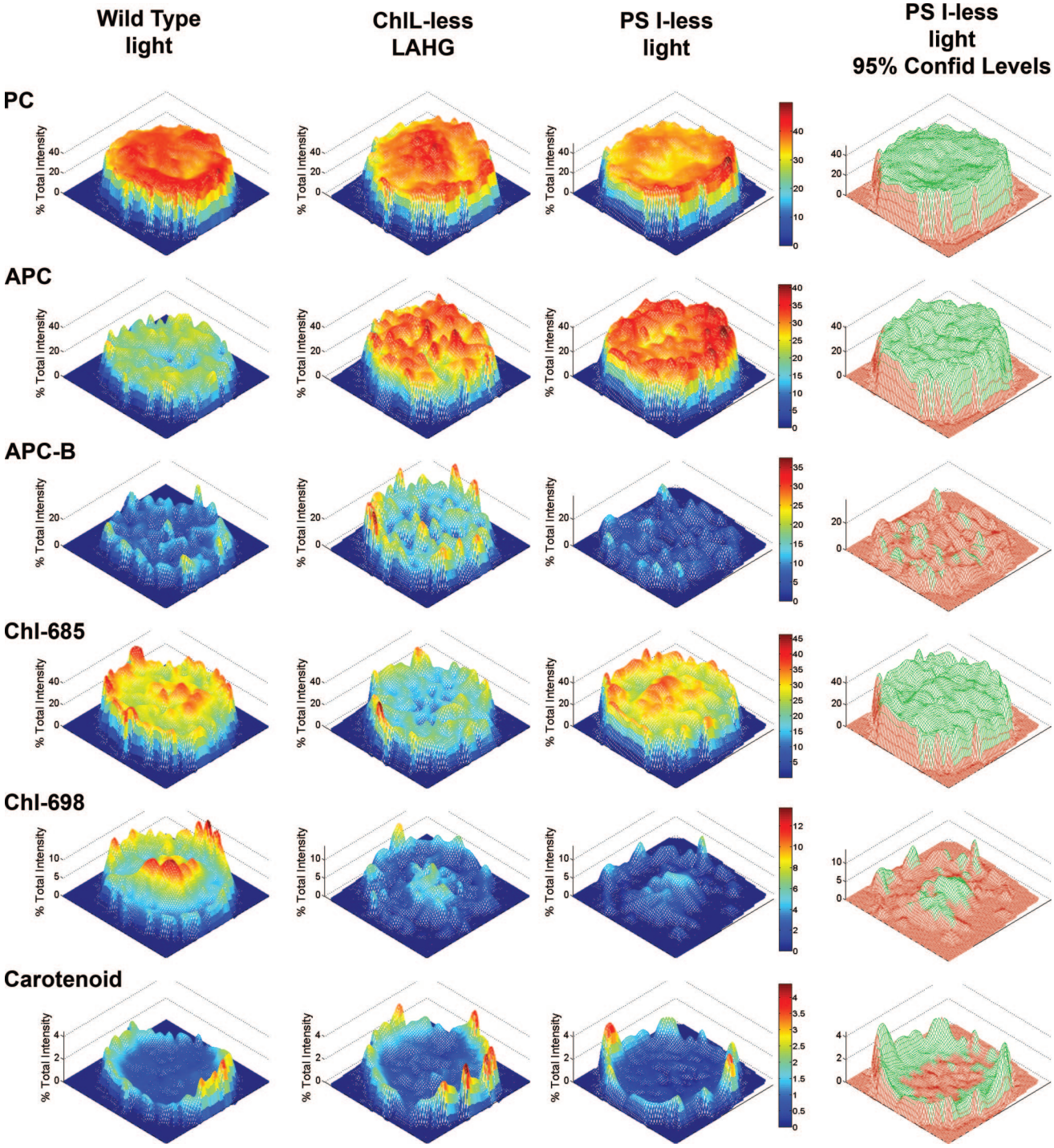

Fig. 3. Mesh plots of percent total intensity per voxel vs. spatial distribution of the six individual components in a wild-type *Synechocystis* cell grown in the light (first column), a ChlL-less cell grown in LAHG conditions (second column), and a PS I-less cell grown in the light (third column). Mesh plots indicating the 95% confidence level for the PS I-less cell are in the fourth column. Voxels in green meet the 95% confidence criterion whereas voxels in red do not. Intensity values were normalized on a per-voxel basis such that the total percent intensity of all components summed to 100. *x* and *y* axis labels have been removed for simplicity. Each of the cells is ≈2 μm in diameter.

Discussion

Localization of Pigments. Hyperspectral fluorescence imaging provides a novel way to localize and identify fluorescent pigments in living cells. Resolved fluorescence components are readily assignable, and the distortion due to energy transfer from phycobilisomes to Chl appears to be small at the high light intensity used because the PC, APC, and APC-B fluorescence localization in wild type and the ChlL-less mutant grown under LAHG conditions was comparable.

While all fluorescence components are present in all cells, the intensity distribution of components across cells is variable (SI Fig. 5). This is consistent with some variation of thylakoid distribution between individual cells as observed in electron microscopy images (2), even though the distribution of thyla-

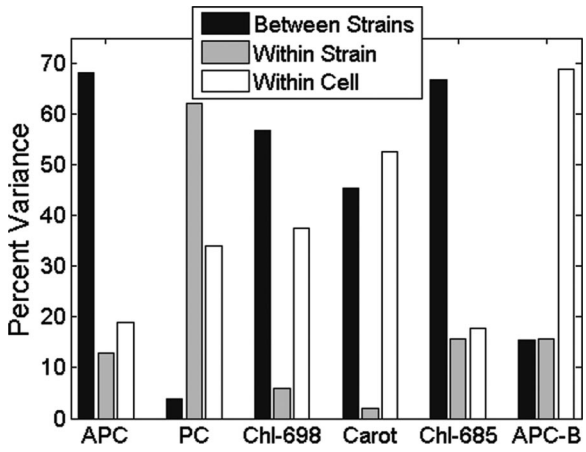

Fig. 4. ANOVA of the emission intensities for each component in the composite image (SI Fig. 5) with 10–12 cells of each strain/condition. The plot presents the percent variance (based on ANOVA results) for each emission component present in the cell.

koids in cells is consistent between strains and growth conditions (SI Fig. 8). Noise observed from weakly fluorescent species (particularly APC-B) that are highly overlapped with more intensely fluorescent components contributed to the heterogeneity, but trends on the larger scale are fully significant (Fig. 3, fourth column).

One example of such a larger-scale trend is the difference in distribution of phycobilins (toward the peripheral thylakoids) vs. Chl-698 (relatively more prevalent toward the center) (Figs. 2 and 3). The data presented here suggest that PS I is enriched in thylakoids toward the center of the cell, whereas phycobilins, which transfer energy primarily to PS II, are associated mostly with the peripheral thylakoids. Significant fluorescence intensity (particularly Chl-698) is observed in the center of cells even though few thylakoids are expected in that location. This is most likely because the center of the cell may have intensity contributions from the inner thylakoid layers above or below the focal plane because of the diffraction-limited resolution in the Z-direction (600 nm) (SI Fig. 10).

Because *Synechocystis* has much more PS I than PS II (31), linear electron transport involving both photosystems and leading to O_2 evolution and production of both NADPH and ATP may be localized along the periphery of the cell. Thylakoids closer to the cell center may be involved more in cyclic electron transfer around PS I, which leads to ATP production but not to net NADP reduction or O_2 evolution.

Carotenoid fluorescence with superimposed resonance-enhanced Raman bands was clearly identified in cells. Although the intensity was weak, it was spectrally distinct from other components. Carotenoids are major pigments in the outer membrane, in the cytoplasmic membrane, and in the thylakoids, explaining the observed halo around the cell and general relative distribution of the carotenoid component (Fig. 3). In contrast, Chl and phycobilisome components are associated only with thylakoids.

Energy Flux and State of Reaction Centers During Illumination. Confocal fluorescence microscopy necessarily involves a high photon flux density. Based on the light intensity used for illumination, approximately half a million quanta hit a specific pigment molecule during the time of illumination (0.24 ms for each voxel). Because ≈0.5% of the light is absorbed by a particular pigment molecule, several thousand quanta will be absorbed in 0.24 ms, corresponding to a quantum being absorbed about every 100 ns. Photosynthetic antennas consist of 100 or more pigment molecules, but the average lifetime of excitations in photosynthetic complexes is <1 ns (11). Therefore, the chance of multiple excitations in an antenna complex during the time of illumination is low. Heating of the sample by absorbed light is not a major issue because we estimate the temperature rise due to absorption of our Gaussian-focused laser beam by Chl to be 0.5 K given our exposure time of 0.24 ms per spectrum and beam parameters (23).

A photosystem excitation rate of ≈1 ns^{-1} implies that P700, the primary donor in the PS I reaction center, is predominantly oxidized during illumination because electron donation to PS I is much slower. Because $P700^+$ and the long-lived P700 triplet state quench fluorescence (38), the PS I Chl fluorescence yield is low under our experimental conditions. Similarly, the PS II Chl fluorescence yield is low because P680, the primary donor in the PS II reaction center, primarily remains in the oxidized state during excitation: $P680^+$, a fluorescence quencher (39), is reduced on the time scale of 10 ns to several microseconds (40), and excitations are expected to arrive at the PS II reaction center 10–1,000 times more frequently.

Hyperspectral confocal fluorescence imaging coupled to MCR analysis provides us with the opportunity to obtain new structural information regarding the distribution and relative concentration of photosynthetic pigments in cyanobacteria. With this new system, fluorescence emission maxima only 10–15 nm apart can be easily distinguished and quantified. The signal-to-noise ratio of the collected data and the quality of the fit between the experimental data and calculated spectra illustrate the confidence with which these multivariate data can be analyzed. In addition, statistical measures to identify the significance of the findings as well as detailed analysis of variance calculations have been made based on the MCR compositional analysis of the hyperspectral images obtained from multiple cells, strains, and growth conditions. Finally, in this study the heterogeneity of the pigment distribution in cells, direct carotenoid visualization (via resonance Raman scattering) in the cell wall and membranes, and preferential location of the two photosystems in cyanobacteria were experimentally observed for the first time *in vivo*.

Materials and Methods

Strains, Culture Conditions, and Electron Microscopy. The *Synechocystis* sp. PCC 6803 mutant strains have been described before (31, 33). Cells were grown in BG-11 medium with 5 mM glucose on a shaker at 30°C at a constant light intensity of 5 μmol of photons per m^2 per second or under LAHG conditions (41). The cell density was ≈5×10^7 cells per milliliter at the time of harvesting. When grown under LAHG conditions, cells were kept in complete darkness for 2 days before the measurement to minimize the Chl content in ChlL-less strains. For electron microscopy, cells were high-pressure-frozen and prepared as described in ref. 2, except that glutaraldehyde was omitted from the freeze-substitution solution. Standard transmission electron microscopy was performed as described in ref. 2.

Hyperspectral Confocal Fluorescence Microscopy. One milliliter of cell suspension was spun down at 300 × *g* for 2 min, the supernatant was discarded, and the cell pellet was resuspended in the remaining liquid. Cells were spotted on an agar-coated microscope slide. A coverslip was applied, and gentle pressure was applied to minimize movement of cells.

Hyperspectral images were acquired with the confocal microscope described in ref. 23. The 488-nm laser emission was focused on the sample, and the fluorescence emission spectrum was recorded from 500 to 800 nm at a rate of 4,200 spectra per second. The spectral resolution varied from 1 nm at 500 nm to 3 nm at 800 nm. The excitation power at the sample was 40 μW, and the exposure time per voxel was 0.24 ms. These settings limited photobleaching during imaging to 10% or less.

Data Analysis. Data analyses were performed on dual-processor desktop computers using in-house Matlab (Mathworks) code with calls to efficient C++ subroutines. A composite image was generated containing raw hyperspectral image data from the centermost slice of 3D images of cells of each strain/condition. Voxels outside the cells were not considered in the MCR

analysis. Principal component analysis of the composite hyperspectral image data weighted for Poisson noise indicated the presence of six independent spectral components from the cells plus one related to the CCD detector. Thus, an initial seven-component MCR model was developed using an equality constraint on the background spectral signature (determined from the analysis of a dark image) and nonnegativity constraints on the spectra and intensities of all other components (23, 25, 26, 28). A procedure including genetic algorithm selection of the most orthogonal spectral channels and spatial voxels was used to achieve the final pure spectral MCR components that were used for all subsequent multivariate analyses. A weighted classical least squares analysis (42) was performed using this final set of pure-component spectra to predict the intensities of the original hyperspectral images, as well as of the composite image.

The noise in the hyperspectral image is from Poisson distributed noise and read noise. The error from these noise sources was determined by reconstructing the composite image from the pure components and their intensities obtained from the weighted classical least squares analysis. Poisson and read noise were added to this noise-free image, and weighted classical least squares was used to predict new intensities. These predicted intensities were compared with the noise-free results to generate prediction errors. This process was repeated 30 times to get an estimate of the error due to the noise. The error was calculated on a per-pixel basis for each component at the 95% confidence level.

ACKNOWLEDGMENTS. We thank Michael Keenan, David Melgaard, and Mark Van Benthem for their contributions to the MCR software and Rachel Noek for performing cross-cut analyses for wild-type cells. Research at Arizona State University was supported by U.S. Department of Energy Contract DE-FG03-01ER15251 (to W.F.J.V.). Sandia is a multiprogram laboratory operated by Sandia Corporation, a Lockheed Martin Company, for the U.S. Department of Energy under Contract DE-ACO4-94AL85000. The Sandia component of this work was funded in part by the U.S. Department of Energy's Genomics: Genomes-to-Life program under the project ''Carbon Sequestration in *Synechococcus* sp.: From Molecular Machines to Hierarchical Modeling.''

1. Blankenship RE (2002) *Molecular Mechanisms of Photosynthesis* (Blackwell Science, Oxford).
2. van de Meene AML, Hohmann-Marriott MF, Vermaas WFJ, Roberson RW (2006) The three-dimensional structure of the cyanobacterium *Synechocystis* sp PCC 6803. *Arch Microbiol* 184:259–270.
3. Tang X-S, Diner BA (1994) Biochemical and spectroscopic characterization of a new oxygen-evolving photosystem II core complex from the cyanobacterium *Synechocystis* PCC 6803. *Biochemistry* 33:4594–4603.
4. Byrdin M, *et al.* (2002) Light harvesting in photosystem I: Modeling based on the 2.5-angstrom structure of photosystem I from *Synechococcus elongatus. Biophys J* 83:433–457.
5. De Weerd FL, Dekker JP, van Grondelle R (2003) Dynamics of β-carotene-to-chlorophyll singlet energy transfer in the core of photosystem II. *J Phys Chem B* 107:6214–6220.
6. Jurgens UJ, Weckesser J (1985) Carotenoid-containing outer membrane of *Synechocystis* sp strain PCC 6714. *J Bacteriol* 164:384–389.
7. Omata T, Murata N (1984) Isolation and characterization of 3 types of membranes from the cyanobacterium (blue-green-alga) *Synechocystis* PCC 6714. *Arch Microbiol* 139:113–116.
8. Gantt E (1981) Phycobilisomes. *Annu Rev Plant Physiol Plant Mol Biol* 32:327–347.
9. MacColl R (1998) Cyanobacterial phycobilisomes. *J Struct Biol* 124:311–334.
10. Elmorjani K, Thomas J-C, Sebban P (1986) Phycobilisomes of wild-type and pigment mutants of the cyanobacterium *Synechocystis* PCC 6803. *Arch Microbiol* 146:186–191.
11. Bittersmann E, Vermaas W (1991) Fluorescence lifetime studies of cyanobacterial photosystem II mutants. *Biochim Biophys Acta* 1098:105–116.
12. Lundell DJ, Yamanaka G, Glazer AN (1981) A terminal energy acceptor of the phycobilisome: The 75,000-dalton polypeptide of *Synechococcus* 6301 phycobilisomes—a new biliprotein. *J Cell Biol* 91:315–319.
13. Gantt E, Conti SF (1969) Ultrastructure of blue-green algae. *J Bacteriol* 97:1486–1493.
14. Nierzwicki-Bauer SA, Balkwill DL, Stevens SE (1983) Three-dimensional ultrastructure of a unicellular cyanobacterium. *J Cell Biol* 97:713–722.
15. Nierzwicki-Bauer SA, Balkwill DL, Stevens SE (1984) The use of high-voltage electron microscopy and semi-thick sections for examination of cyanobacterial thylakoid membrane arrangements. *J Microsc* 133:55–60.
16. Jordan P, *et al.* (2001) Three-dimensional structure of cyanobacterial photosystem I at 2.5 angstrom resolution. *Nature* 411:909–917.
17. Loll B, Kern J, Saenger W, Zouni A, Biesiadka J (2005) Towards complete cofactor arrangement in the 3.0 angstrom resolution structure of photosystem II. *Nature* 438:1040–1044.
18. Sherman DM, Troyan TA, Sherman LA (1994) Localization of membrane proteins in the cyanobacterium *Synechococcus* sp PCC 7942: Radial asymmetry in the photosynthetic complexes. *Plant Physiol* 106:251–262.
19. Joshua S, Bailey S, Mann NH, Mullineaux CW (2005) Involvement of phycobilisome diffusion in energy quenching in cyanobacteria. *Plant Physiol* 138:1577–1585.
20. Mullineaux CW (1994) Excitation-energy transfer from phycobilisomes to photosystem I in a cyanobacterial mutant lacking photosystem II. *Biochim Biophys Acta* 1184:71–77.
21. Mullineaux CW, Tobin MJ, Jones GR (1997) Mobility of photosynthetic complexes in thylakoid membranes. *Nature* 390:421–424.
22. Wolf E, Schussler A (2005) Phycobiliprotein fluorescence of *Nostoc punctiforme* changes during the life cycle and chromatic adaptation: Characterization by spectral confocal laser scanning microscopy and spectral unmixing. *Plant Cell Environ* 28:480–491.
23. Sinclair MB, Haaland DM, Timlin JA, Jones HDT (2006) Hyperspectral confocal microscope. *Appl Optics* 45:3283–3291.
24. Bro R, DeJong S (1997) A fast non-negativity-constrained least squares algorithm. *J Chemometr* 11:393–401.
25. Keenan MR, Kotula PG (2004) Accounting for Poisson noise in the multivariate analysis of ToF-SIMS spectrum images. *Surf Interface Anal* 36:203–212.
26. Kotula PG, Keenan MR, Michael JR (2003) Automated analysis of SEM X-ray spectral images: A powerful new microanalysis tool. *Microsc Microanal* 9:1–17.
27. Timlin JA, *et al*. (2005) Hyperspectral microarray scanning: Impact on the accuracy and reliability of gene expression data. *BMC Genomics* 6:72.
28. Van Benthem MH, Keenan MR, Haaland DM (2002) Application of equality constraints on variables during alternating least squares procedures. *J Chemometr* 16:613–622.
29. Ikeuchi M, Tabata S (2001) *Synechocystis* sp PCC 6803: A useful tool in the study of the genetics of cyanobacteria. *Photosynth Res* 70:73–83.
30. Vermaas W (2004) Targeted genetic modification of cyanobacteria: New biotechnological applications. *Handbook of Microalgal Culture*, ed Richmond A (Blackwell Science, Oxford), pp 457–470.
31. Shen G, Boussiba S, Vermaas WFJ (1993) *Synechocystis* sp PCC 6803 strains lacking photosystem I and phycobilisome function. *Plant Cell* 5:1853–1863.
32. Suzuki JY, Bauer CE (1992) Light-independent chlorophyll biosynthesis: Involvement of the chloroplast gene *chlL* (*frxC*). *Plant Cell* 4:929–940.
33. Wu Q, Vermaas W (1995) Light-dependent chlorophyll *a* biosynthesis upon *chlL* deletion in wild-type and photosystem I-less strains of the cyanobacterium *Synechocystis* sp PCC 6803. *Plant Mol Biol* 29:933–945.
34. He Q, Brune D, Nieman R, Vermaas W (1998) Chlorophyll *a* synthesis upon interruption and deletion of *por* coding for the light-dependent NADPH: Protochlorophyllide oxidoreductase in a photosystem-I-less/*chlL*$^-$ strain of *Synechocystis* sp. PCC 6803. *Eur J Biochem* 253:161–172.
35. Andreeva A, Velitchkova M (2005) Resonance Raman spectroscopy of carotenoids in Photosystem I particles. *Biophys Chem* 114:129–135.
36. Tracewell CA, Cua A, Bocian DF, Brudwig GW (2005) Resonance Raman spectroscopy of carotenoids in Photosystem II core complexes. *Photosynth Res* 83:45–52.
37. Gill EM, Wittershaus BP (1999) Spectral resolution of low-energy chlorophylls in Photosystem I of *Synechocystis* sp PCC 6803 through direct excitation. *Photosynth Res* 61:53–64.
38. Schlodder E, Cetin M, Byrdin M, Terekhova IV, Karapetyan NV (2005) $P700^+$- and $^3P700$-induced quenching of the fluorescence at 760 nm in trimeric Photosystem I complexes from the cyanobactenium *Arthrospira platensis. Biochim Biophys Acta* 1706:53–67.
39. Bruce D, Sampson G, Carpenter C (1997) The origins of non-photochemical quenching of chlorophyll fluorescence in photosynthesis. Direct quenching by $P680^+$ in photosystem II enriched membranes at low pH. *Biochemistry* 36:749–755.
40. Kuhn P, Eckert H, Eichler HJ, Renger G (2004) Analysis of the $P680^+$ reduction pattern and its temperature dependence in oxygen-evolving PSII core complexes from a thermophilic cyanobacteria and higher plants. *Phys Chem Chem Phys* 6:4838–4843.
41. Anderson SL, McIntosh L (1991) Light-activated heterotrophic growth of the cyanobacterium *Synechocystis* sp strain PCC 6803: A blue-light-requiring process. *J Bacteriol* 173:2761–2767.
42. Haaland DM, Easterling RG (1982) Application of new least-squares methods for the quantitative infrared-analysis of multicomponent samples. *Appl Spectrosc* 36:665–673.